Colloids and Surfaces A: Physicochemical and Engineering Aspects 711 (2025) 136410

Contents lists available at ScienceDirect

Colloids and Surfaces A: Physicochemical and Engineering Aspects

journal homepage: www.elsevier.com/locate/colsurfa

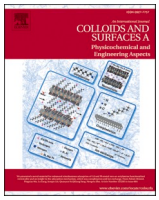

Acoustically driven vertical coalescence of liquid marbles

Aditya Vashi *, Ajeet Singh Yadav, Navid Kashaninejad, Nam-Trung Nguyen

Queensland Micro and Nanotechnology Centre, Griffith University, 170 Kessels Road, Nathan, Queensland 4111, Australia

GRAPHICAL ABSTRACT

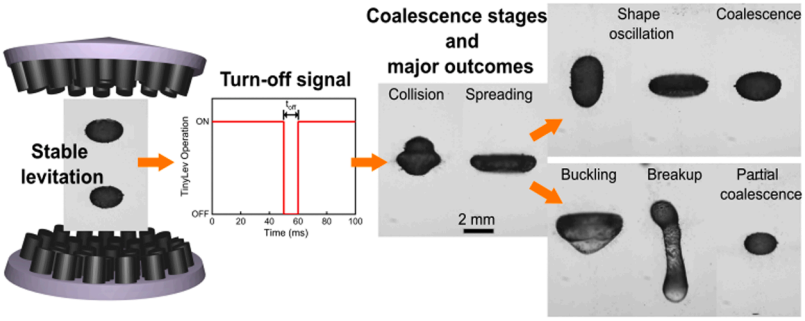

ARTICLE INFO

Keywords:
Acoustic levitation
Liquid marbles
Vertical coalescence
Contactless manipulation

ABSTRACT

Liquid Marbles (LMs) are liquid droplets coated with a shell of micro- or nanoparticles. These versatile structures hold promise for diverse applications, including microreactors, gas sensors, and fluid pumps. Consequently, various strategies have been explored to manipulate LMs in terms of transportation, coalescence, and separation. Among these strategies, acoustic levitation presents a unique opportunity for surface-free manipulation of LMs. This paper introduces a simple and cost-effective method to achieve the head-on coalescence of LMs using acoustic levitation. Coalescence was accomplished by superimposing a control signal on continuous acoustic fields to facilitate collision and merging. Five distinct outcomes were identified, which depended on the ability of the acoustic levitator to hold and merge the resultant liquid marble. The results revealed a significant influence of acoustic pressure in the major outcomes of complete coalescence and partial coalescence after the collision. Our experimental results provide deeper physical insights into contactless head-on LM coalescence while demonstrating its feasibility as an initial step toward advanced LM manipulation techniques using acoustic levitation.

1. Introduction

Levitation is a technique to counteract gravity. Levitation has gained popularity due to recent advances in science and technology [1]. Levitation provides a contactless environment and condition similar to outer space, eliminating heterogeneous nucleation and preventing cross-contamination with surfaces [2]. Among the levitation methods, acoustic levitation can suspend any material without the need for a specific physical property [3]. Therefore, acoustic levitation has found applications in material synthesis [4], analytical chemistry [5],

* Corresponding author.
E-mail address: aditya.vashi@griffithuni.edu.au (A. Vashi).

https://doi.org/10.1016/j.colsurfa.2025.136410
Received 9 December 2024; Received in revised form 20 January 2025; Accepted 10 February 2025
Available online 11 February 2025

pharmacy [6], microgravity research [7], and rheology [8]. The most common way to realise acoustic levitation is utilising a standing wave, where objects can be levitated at low-pressure regions known as nodes [9]. Standing waves can be generated with two main configurations: resonant [9] and non-resonant [10]. In a resonant levitator, standing waves are created by carefully tuning the distance between the acoustic transducer and the reflector. In contrast, non-resonant levitators have transducers on both sides of the working space, removing the need for frequency tuning.

Due to the contactless environment and the freedom in material selection, acoustic levitation has been emerging as a novel tool to perform fluid manipulation such as transportation, coalescence, and oscillation of droplets [11,12]. Among the fluid manipulation techniques, coalescence is the process where two or more entities merge to form a single entity and is ubiquitous in many natural phenomena, such as raindrop formation [13], ocean mist production [14], and atmospheric aerosol circulation [15]. In addition, coalescence plays a significant role in industrial processes, including ink-jet printing [16], spray cooling [17], sintering in metallurgy [18], and emulsification [19]. Foresti et al. demonstrated the first contactless coalescence concept with acoustic levitation [20]. The team arranged discretised planar Langevin piezoelectric transducers (LPTs) with a single reflector at a uniform distance [20]. Droplets were transported and coalesced by controlling the LPTs individually [20]. Instead of LPTs, Abe et al. implemented phased arrays and modulated them to create two focal points where droplets can be levitated [21]. Reducing the length between two focal points, resulting in lateral coalescence of droplets. The team also demonstrated the same concept of reduced gravity in later works [22,23]. However, lateral coalescence with the multi-axis levitation approach requires a complex setup, significant space, and high experimental skills. Beyond lateral coalescence, Brotton et al. demonstrated head-on coalescence via large-amplitude axial oscillation in a single-axis resonant levitator [24]. Although this group achieved contactless controlled chemistry through droplet oscillation, understanding head-on coalescence dynamics with this approach remains challenging due to limited control over the merging process of the droplets. Recently, our group has achieved head-on coalescence by simply superimposing a turn-off signal in a single-axis non-resonant device [25]. This method is cost-effective, less complex, easy to implement, and requires minimal space. Additionally, controlling the turn-off period of the signal allows for efficient visualisation of coalescence dynamics. However, the challenge remains to achieve full coalescence of bare water droplets due to surface instability in the acoustic field.

Over the past two decades, liquid droplets encapsulated with micro or nanoscale hydrophobic or oleophobic powder known as liquid marbles (LMs) have gained attraction due to their non-wetting property [26]. The layer of powder on the droplet surface allows LMs to move freely on a solid substrate, float [27] or sink [28] in a liquid while maintaining its integrity. Non-wetting property, freedom of moving, and permeable particle layer enabled an LM to serve as a microreactor [29], pump [30], and gas sensor [31]. Effective manipulation of LMs is a fundamental step toward practical applications. Therefore, researchers have established multiple manipulation schemes for LMs [32,33]. Particle properties play a crucial role in the manipulation of LMs, as factors such as particle size, structure, and roughness significantly influence the behaviour of the droplet interface [34–36]. To form the liquid bridge and drive the coalescence of LMs, it is important to remove the particle barrier. In lateral coalescence, this liquid-liquid contact is formed using external forces such as magnetic [37], electric [38], or centrifugal [39] force. While in vertical coalescence, LM is dropped from a certain height onto a stationary LM [40]. When the impact velocity exceeded a threshold, the resulting deformation of the LMs caused particle displacement from the contact area, enabling liquid-liquid contact and facilitating LM coalescence [41]. Although these methods have proven effective for LM coalescence, none of the methods are contact-free and carried out on the surface.

Chen et al. first-time demonstrated the contact-free coalescence of LMs using acoustic levitation [42]. The lateral coalescence was attained by simply positioning the LMs side by side and levitating them with a copper sieve [42]. The team observed that at a lower acoustic pressure, both LMs remained separately levitated, while higher acoustic pressure induced their coalescence. However, the critical acoustic pressure at which LMs merged is still unclear and requires further insights. The coalescence of LMs requires extra energy to overcome the particle barrier for merging to occur. Moreover, these particle layers may offer surface stability from external acoustic forces which initiated multiple surface instabilities in bare droplets during coalescence [25]. However, the understanding of surface instabilities for LMs during the coalescence also remains unclear to date. Therefore, it is interesting to achieve contact-free LMs coalescence with different methods, which provides a better understanding of LMs coalescence dynamics in acoustic levitation.

In this paper, we experimentally demonstrated for the first time the head-on coalescence of LMs in acoustic levitation, utilising our method of controlled releasing and catching. We varied LMs volumes, turn-off time, and acoustic pressure in terms of driving voltage to characterise head-on LMs coalescence in acoustic levitation. As this study represents the first demonstration of vertical coalescence in acoustic levitation, our primary objective was to validate the feasibility of the coalescence process. Therefore, we did not vary the particle properties for this study. Our approach offers cost-effective and less complex way to achieve LMs coalescence with acoustic levitation, paving the way for contactless chemical or biochemical reactions while providing a novel framework for surface-free digital microfluidics applications.

2. Materials and method

2.1. Materials and LM preparation

Each LM was prepared manually and separately, according to the requirements of the subsequent experiments. Fig. 1a illustrates sequential stages for the preparation of LMs. At first, a deionised (DI) water droplet was released on a polytetrafluoroethylene (PTFE) (Sigma-Aldrich, nominal diameter of 1 μm) powder bed. Various water volumes were utilised in the experiments to evaluate the effect of size on the coalescence of LMs. Droplet volumes of 5, 6 and 7 μl were dispensed with a micropipette (Eppendorf Research plus – 3123000039, volume range from 1 to 20 μl). Droplet volumes of 3 and 4 μl were dispensed using a smaller micropipette (Eppendorf Research LLG 9280001, volume range from 0.5 to 10 μl).

After dispensing, the liquid droplet was rolled on the powder bed by turning and shaking until its surface was covered thoroughly with a layer of microparticles, Fig. 1a. The formation of LMs with this method can be elucidated by the concept of surface energy minimisation [43]. The mechanically stable LM was transferred from the powder bed to a stainless-steel sieve using a spatula, Fig. 1a. The sieve, with a LM on it, was then carefully moved to the designated node position for levitation. The stainless-steel sieve facilitated the propagation of sound waves, enabling efficient levitation of the LM.

2.2. Experiment setup and coalescence procedure

Fig. 1b depicts the experimental setup. The acoustic levitator 'TinyLev' was employed for contact-free levitation of the LMs [44]. The TinyLev operated at 40 kHz, which corresponds to a sound wavelength (λ) of 8.58 mm. The signal was excited through nano Arduino and amplified by L297N dual H-bridge stepper motor driver. Both devices were powered by a variable DC power supply (Keithley 2200–30–5). The acoustic pressure in the levitator was varied by changing the voltage from the power supply [7]. Voltages of 10, 10.5, and 11 V were used to characterise the effect of acoustic power on the coalescence of LMs.

Following the activation of the levitator, the prepared LMs were

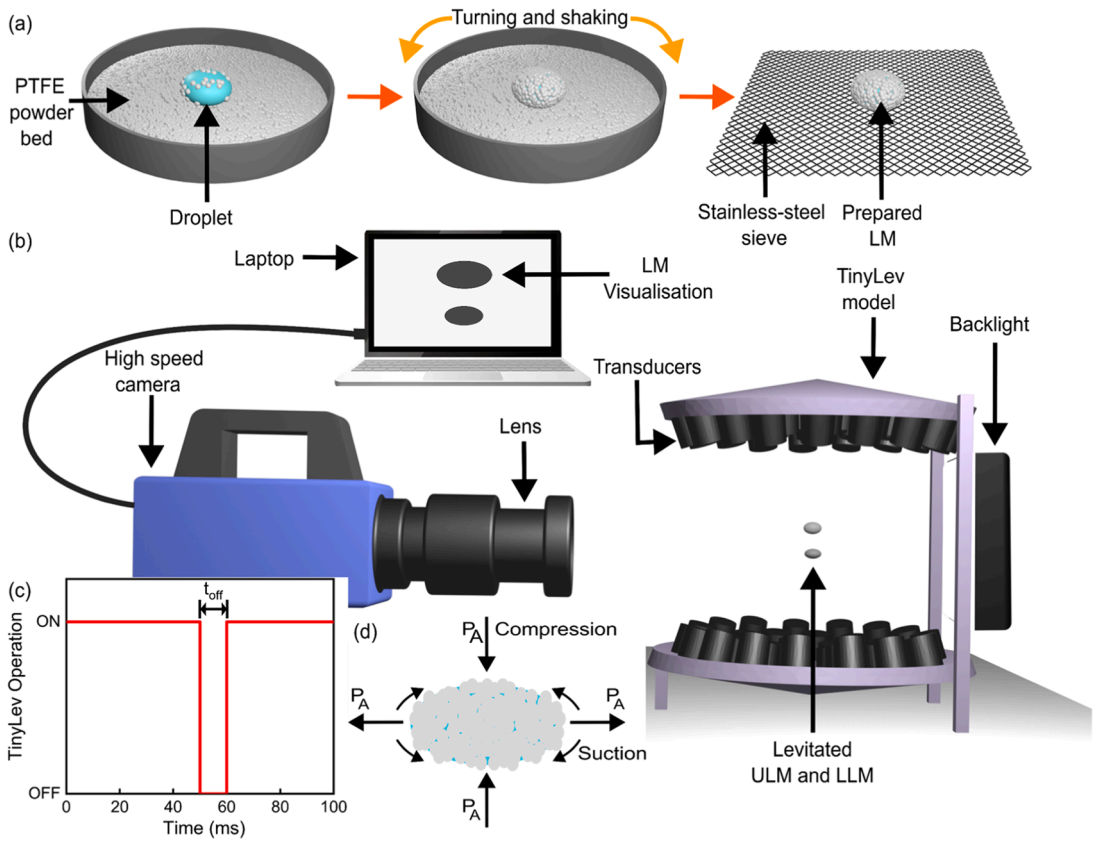

Fig. 1. (a) Preparation of liquid marble. (b) Experiment setup for LM coalescence. (c) Turn-off signal to interrupt the acoustic field, allowing the liquid marbles to fall freely for a short period. (d) Acoustic radiation pressure on LM.

precisely levitated at two consecutive nodes in the centre of the levitator cavity, Fig. 1b. LMs were levitated individually using a consistent protocol. First, the sieve holding the LM was carefully brought near the upper node. Once positioned close to the node, the LM automatically moved to the node due to the low-pressure region, achieving successful levitation. Since the LM does not adhere to the sieve, the sieve could be removed from acoustic cavity without concern. After the stable levitation of the LM at the upper node, the second LM was introduced at the lower node using the same method. Although this process was smooth and efficient, disruptions occasionally occurred, such as the LM wetting the sieve due to improper packing or an LM falling into the cavity. In such cases, the LMs were discarded, and new LMs were prepared and levitated following the same protocol. The LM levitated at the upper node was designated as the Upper Liquid Marble (ULM), and the below LM was designated as the Lower Liquid Marble (LLM), Fig. 1b. Sizes of ULM and LLM were varied by preparing LM from different droplet volumes. ULM was prepared with droplet volumes 5,6 and 7 μl and LLM was prepared with droplet volumes 3 and 4 μl.

Upon the stable levitation of both LMs, we superimposed a turn-off signal to the continuous acoustic signal to achieve the coalescence of LMs, Fig. 1c. The turn-off signal was introduced through an additional Arduino UNO controller. The circuit diagram for generating the turn-off signal can be referenced from our previous article [25]. The LM coalescence was recorded at 2000 fps using a high-speed camera (Photon Fastcam SA3) with a Nikon micro lens (AF Micro-NIKKOR 60 mm f/2.8D), Fig. 1b. A White LED light source was positioned at the rear side of the levitator to enhance the quality of the image, Fig. 1b.

2.3. Properties of the liquid marbles

The layer of microparticles on the core liquid affect surface tension and density of the core liquid [45]. The effective surface tension (σ_m) of LM can be described as:

$$\sigma_m = \sigma_l + \sigma_{\text{int}} \tag{1}$$

where σ_l is the surface tension of the pure liquid and σ_{int} is the modifying parameter, which depends on the intramolecular force between liquid and particle and can be positive or negative [45]. Additionally, various methods have been investigated for the direct measurement of LM effective surface tension [46]. In our study, we used 1-μm PTFE particles. Arbatan and Shen employed capillary rise method to measure the effective surface tension of LM, using 1-μm PTFE particles and DI water as liquid core, with droplet sizes ranging from 30 – 300 μl [47]. In their study, measured effective surface tension was closed to that of DI water [47]. Therefore, in our study, we considered the effective surface tension equivalent to that of DI water, which is 0.073 N/m.

The effective density of LMs may be evaluated by the following correlation [48],

$$\rho_m = \frac{D^3\rho + 3.45nD^2 d_p\rho_p}{(D + 2nd_p)^3} \tag{2}$$

Where D and ρ are the diameter and density (0.998 gm/ml) of DI water, while d_p and ρ_p are the diameter (1 μm) and density (2.15 gm/ml at 25 °C) of microparticles. Parameter n denotes the number of microparticle's layers covering the DI water, which is between 3 and 5 [48]. Using this equation and assuming a droplet diameter of 2 mm and 4 layers of microparticles, the density value is ρ_m= 1 gm/ml, which closely approximates the density of water. As a result, we kept the effective density equivalent to DI water throughout the calculations.

2.4. Shape of the LM in acoustic field

LM experiences acoustic radiation pressure on the surface when levitated in acoustic field. The exerted acoustic radiation pressure on the surface can be calculated according to King's theory [49],

$$P_A = \frac{1}{2\rho_0 c_0^2} < p^2 > - \frac{1}{2}\rho_0 < v^2 > \quad (3)$$

where, p and v are the sound pressure and particle velocity, ρ_0 density of medium air, c_0 is the sound velocity in air. $< >$ denotes the time average over period of acoustic oscillation. The distribution of acoustic radiation pressure over the surface is not uniform. It is positive (compression) at polar area and negative (suction) at the equator, Fig. 1d [50,51]. This causes the LM to adapt an ellipsoidal shape, which can be adjusted by varying the sound pressure, Fig. 1d. In TinyLev, sound pressure can be varied by changing the driving voltage (U). The sound pressure at point r from one transducer can be calculated by [52],

$$p(\mathrm{r}) = p_0 U\left((D_\mathrm{f}(\theta)/d)\mathrm{e}^{\mathrm{i}(\varphi+kd)}\right) \quad (4)$$

where, p_0 is a constant that define transducer output efficiency, D_f is the directivity function which depends on the angle θ between the transducer normal and the point r, d is the propagation distance in space, φ is the emitting phase of the source, and k is the wave number. The sound pressure generated by TinyLev is the combined result of the sound pressure contributions from each individual transducer. The comprehensive study of sound pressure and its effect on levitated object can be found in our previous work [7].

2.5. Determination of LM energies and impact velocity

Evaluating the surface energy and kinetic energy of LMs is important to understand the dynamics of their coalescence. Surface energy (E_s) of LM is:

$$E_s = \sigma_m S \quad (5)$$

Where S represents the surface area of the LM, which depends on its shape. A LM has the shape of an ellipsoid, with a rotational symmetry along the vertical axis (oblate spheroid). We first measured horizontal (a_{hor}) and vertical (a_{ver}) radius using ImageJ (National Institute of Health, United States) as an analysis tool. Next, the surface area of the LM was measured by rotating the elliptical curve around the vertical axis.

The kinetic energy (E_k) of a LM is expressed as,

$$E_k = \frac{1}{2}\rho_m V v^2 \quad (6)$$

Where V represents the volume (same as dispensed droplet volume) of LM and v denotes the velocity of the LM. The velocity data were extracted using Droplet Morphometry and Velocimetry (DMV) software [53].

While we could extract impact velocity from the DMV, the varying impact times of the LMs would make the evaluation process time-consuming. In addition, we encountered the problem of separating the edge detection of ULM and LLM near impact due to their closeness. Therefore, we manually calculated impact velocity (v_i) using the following equation,

$$v_i = \frac{\sqrt[2]{(x_1 - x_2)^2 + (y_1 - y_2)^2}}{t_1 - t_2} \quad (7)$$

Where (x_1, y_1) is the centroid coordinate of the droplet at impact, (x_2, y_2) is centroid coordinate of the droplet at 2 frames before impact, and t_1 and t_2 are corresponding times. The centroid coordinates for Eq. 7 were measured using ImageJ tool.

3. Results and discussions

3.1. Classification and temporal evolution of outcomes after applying turn-off signal

After turning off the transducers, we observed five distinct impact outcomes. The outcomes were distinguished based on the holding and coalescence ability of ULM and LLM in the acoustic cavity as shown in Fig. 2a. Each outcome was represented as a number from 1 to 5. Outcome 1 took place when the LMs did not merge but maintained their position within the acoustic cavity after applying a turn-off signal (Supplementary Video 1). In outcome 2, both LMs merged completely and stayed in the cavity post-coalescence (Supplementary Video 2). As with outcome 2, LMs coalesced and remained levitated for outcome 3. However, during the coalescence the merged LM partially disintegrated, leading to a loss of liquid (Supplementary Video 3). Contrary to outcomes 1, 2, and 3, outcomes 4 and 5 resulted in the LMs failing to maintain their levitated positions. In outcome 4 (Supplementary Video 4), the LMs coalesced before falling into the cavity, while in outcome 5 (Supplementary Video 5), they fell without coalescing.

Supplementary material related to this article can be found online at doi:10.1016/j.colsurfa.2025.136410.

Fig. 2b illustrates the time evolution of the outcomes through a sequence of images. In Fig. 2b, the volumes of ULM and LLM were 6 μl and 4 μl, respectively. Different outcomes occurred by varying the period of the turn-off signal. These values are shown in the Fig. 2b next to outcome numbers. Notably, outcomes 2 and 3 occurred at a similar turn-off period. The possible reasons for this variation are elaborated in Sections 3.2 and 3.3. Both LMs were levitated at 10 V to their respective node, Fig. 2b at 0 ms. Introducing the turn-off signal caused the acoustic pressure in the cavity to cease. As a result, both LMs commenced falling downward under the influence of gravity, converting gravitational potential energy into kinetic energy as shown at 10 ms in Fig. 2b. Reintroducing the signal restored the acoustic pressure in the cavity. Interestingly, though the applied turn-off signal was between 13 and 16 ms, both LMs continued to move downward, Fig. 2b at 20 ms. This behaviour was consistent for all outcomes. The reason was the acquired kinetic energy of LMs, which resist the acoustic pressure in the cavity. After 20 ms, each outcome exhibited different behaviour at various times. The time evolution of each outcome is displayed as a vertical time sequence of images in Fig. 2b.

For outcome 1, the reintroduction of acoustic pressure successfully counteracts the kinetic energy of both LMs. Consequently, both LMs reversed their direction and moved upwards to obtain their original position at the low-pressure node, Fig. 2b at 30 ms of outcome 1. However, before securing the node position, both LMs dissipated acquired energy through vertical oscillation in the cavity, which became evident for outcome 1 at 70 and 90 ms in Fig. 2b. At last, both LMs regained their node position without coalescing with each other, Fig. 2b at 1.5 s of outcome 1. In outcome 2, once the acoustic signal turned on, ULM continued to descend, resisting acoustic pressure. On the other hand, LLM ascended, which resulted in the collision of both LMs, Fig. 2b at 35 ms of outcome 2. Due to impact, PTFE-coated particles moved away from the contact area, leading to the occurrence of liquid-liquid contact and merging of two LMs into a single marble [41]. Merged LM spread horizontally giving rise to surface energy by dissipating kinetic energy, Fig. 2b at 40 ms of outcome 2. After maximum spreading, LM retracted to minimise the surface energy. Due to reduction in surface area of the marble, particle accumulates on each other. Particles away from the liquid surface had weak bonding with the liquid. Moreover, particles were directly exposed to external acoustic streaming in the cavity [42]. As a result, coating microparticles detached from the coalesced LM as visible at 50 ms of outcome 2 in Fig. 2b. For outcome 2, after the collision, the merged LM went through multiple spreading and retraction phases to dissipate energy before regaining the node position shown in Fig. 2b at 240 ms of outcome 2.

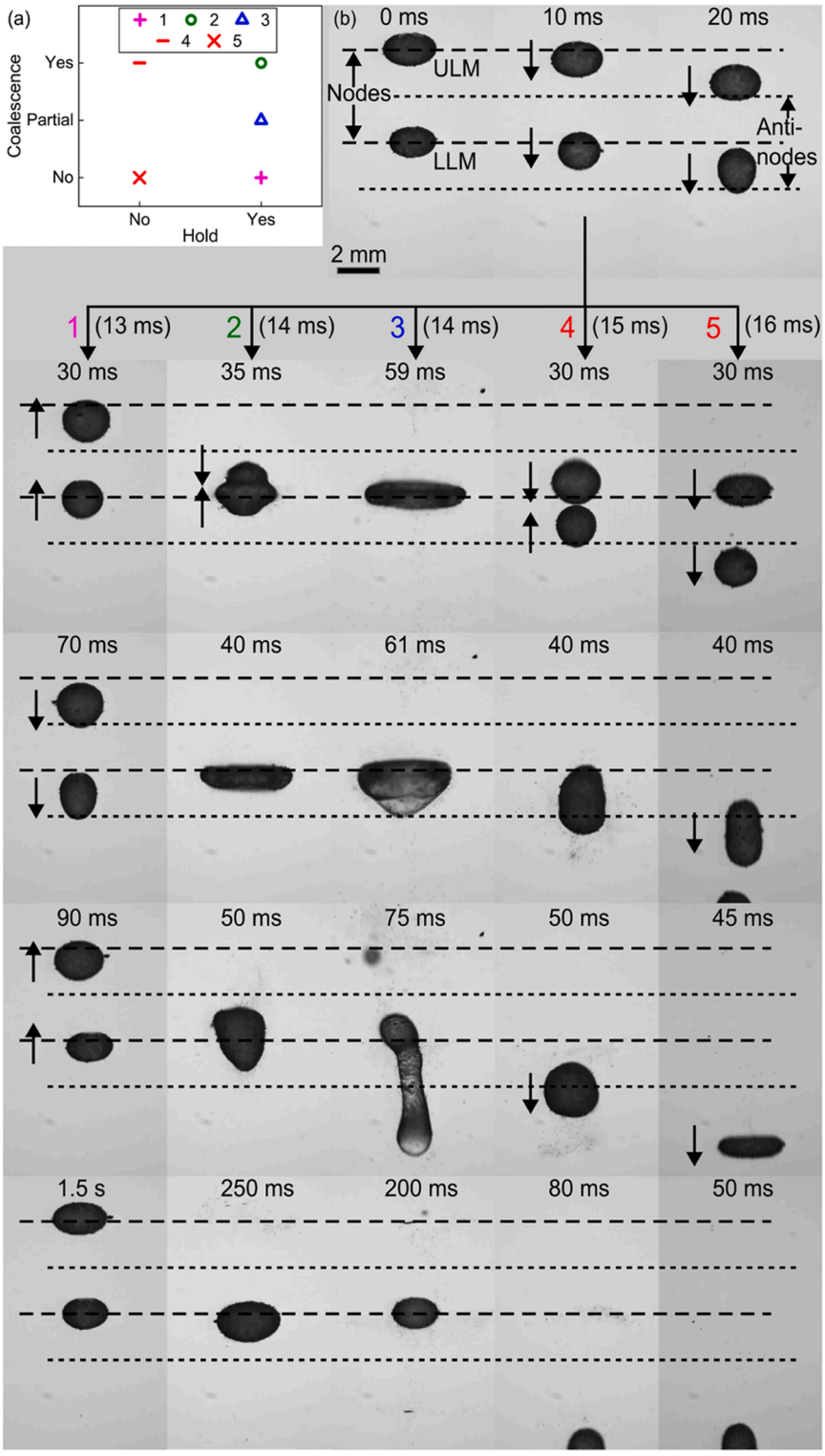

Fig. 2. (a) Classification of outcomes based on holding and merging ability of LMs. (b) Temporal evolution of different outcomes after applying the turn-off signal. Before applying the turn-off signal, ULM and LLM were stably levitated at consecutive node. Different outcomes observed at different turn-off time, keeping the voltage and LMs volume similar. Turn-off time for each outcome is displayed next to outcome numbers.

Collision of ULM and LLM occurred for outcome 3 after applying the turn-off signal. However, we observed buckling instability in outcome 3. In our previous study, we reported that higher spreading width caused the merged droplet to buckle [25]. In Fig. 2b, spreading and buckling events for outcome 3 are shown at 59 ms and 61 ms, respectively. Buckling led to the abrupt closure of the LM, which resulted in its breakup, Fig. 2b at 75 ms of outcome 3. The remaining partial droplet stayed levitated at the node, Fig. 2b at 200 ms of outcome 3.

Similar to outcome 2 and 3, in outcome 4, ULM descended while LLM ascended, Fig. 2b at 30 ms of outcome 4, leading to the coalescence of LMs after the reintroduction of acoustic pressure, Fig. 2b at 40 ms of outcome 4. However, the acoustic pressure was unable to hold the

merged droplet, which continued to move downward and eventually dropped in the acoustic cavity, as shown at 50 and 80 ms of outcome 4 in Fig. 2b. For outcome 5, both LMs resisted the acoustic pressure and continued their downward movement, ultimately falling into the acoustic cavity without coalescence. The time evolution of outcome 5 is shown at 30, 40, 45, and 50 ms in Fig. 2b.

3.2. Effect of t_{off} time on the outcomes

Examining the temporal evolution made clear that changing the period t_{off} caused the different outcomes. In addition, the first 30 ms after applying turn-off signal played an important role in deciding the movement of both LMs. Therefore, we evaluated the displacement from node positions, surface and kinetic energies of LMs over the first 30 ms. To investigate the effect of the period t_{off}, the driving voltage (10 V), volumes of ULM (6 μl), and LLM (4 μl) were kept similar with parameters used in the previous section.

Figs. 3a and 3b shows the respective kinetic energies of ULM and LLM over the first 30 ms for different outcomes. Turn-off period of each outcome is indicated in Fig. 3a. The kinetic energies of both ULM and

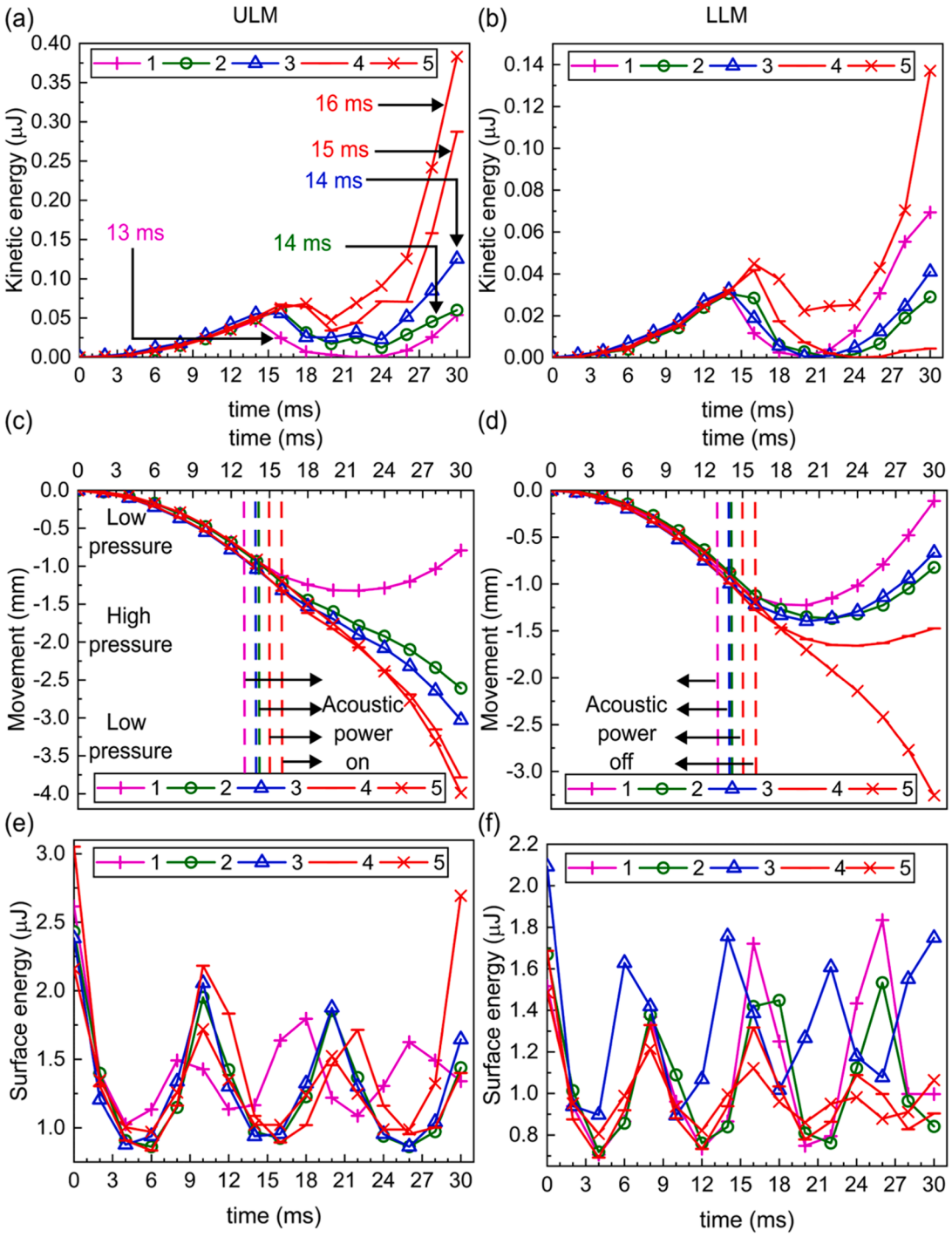

Fig. 3. Variation in kinetic energies of (a) ULM and (b) LLM at different t_{off} periods for different outcomes over first 30 ms. (c) ULM and (d) LLM movement from the respective node position (0 mm) at different t_{off} time for different outcomes over first 30 ms. (e) ULM and (f) LLM variation in surface energies at different t_{off} time for different outcomes over first 30 ms. 0 ms represents the time at which turn-off signal is applied.

LLM increased during the turn-off period, Figs. 3a and 3b. For 13 ms t_{off}, the kinetic energy of ULM increased up to 0.05 μJ while the kinetic energy of LLM increased until 0.03 μJ, Fig. 3a and b. The rate of change in kinetic energy of ULM was higher compared to LLM due to the higher mass of ULM. The kinetic energy of outcome 2 and 3 whose t_{off} period was 14 ms surged by approximately 0.06 μJ for ULM and 0.035 for LLM, Fig. 3a and b. Increasing the turn-off period to 15 ms resulted in a rise in kinetic energy for both ULM and LLM, as observed in Fig. 3a and b for outcome 4. The highest increase in kinetic energy was recorded before the signal was turned on for outcome 5 at a 16 ms turn-off duration, with values of approximately 0.08 μJ and 0.05 μJ for the ULM and LLM, respectively (Fig. 3a and b). During the turn-off period, both ULM and LLM moved downward from the node position as shown in Fig. 3c and d and explained in the above section. ULM descended between 1.0 and 1.5 mm, while LLM descended between 0.75 – 1.25 mm for all outcomes, Fig. 3c and d.

Once the acoustic signal was turned on, both ULM and LLM were exposed to acoustic pressure. As a result, kinetic energy of both LMs decreased, Fig. 3a and b. For $t_{off} = 13$ ms, kinetic energy dropped as low as 0.0002 μJ for ULM and LLM. The decrease in kinetic energy was reflected in the movement of LMs and descended only around 0.2 mm after the reintroduction of the signal, Fig. 3c and d. As the kinetic energy almost reached zero, both LMs could not resist acoustic pressure and attempted to acquire the original position at low pressure and move upward, as shown in Fig. 3c and d. As the LMs moved from high pressure to low pressure, their kinetic energies increased again, as clearly observed in Fig. 3a and b after 22 ms and 20 ms for ULM and LLM, respectively, at 13 ms off.

For 14-ms turn-off duration, the kinetic energy of ULM reduced to 0.012 μJ for outcome 2 and 0.022 μJ for outcome 3, Fig. 3a. The energy continued to reduce until 24 ms, and during this period, ULM descended around 2 mm from the node position for both outcomes, Fig. 3c. This position was slightly below the high-pressure region. Therefore, ULM continued to descend resisting acoustic pressure at the low-pressure region of the second node, where LLM was levitated, Fig. 3c. Additionally, the kinetic energy also increased due to the movement from high pressure to low pressure, Fig. 3a. Contrary to ULM, the kinetic energy of LLM for outcomes 2 and 3 decreased to around 0.0003 μJ, which led to the same behaviour as outcome 1 and LLM moved upward, Fig. 3b. Consequently, collision of ULM and LLM took place which resulted in coalescence or partial coalescence. Interestingly, the LMs of outcome 3 had a higher kinetic energy than the ULM and LLM of outcome 2, Fig. 3a and b. Possible reason is the varying acoustic pressure at different positions within the levitator. Due to the higher kinetic energy, coalesced LM spread more and resulted in buckling.

Same as for 13 and 14 ms turn-off time, the kinetic energy of ULM decreased for $t_{off} = 15$ ms and $t_{off} = 16$ ms once the turn-off duration is over. However, the reduction of kinetic energy for ULM was less compared to 13 and 14 ms turn-off period. The recorded minimum kinetic energy was 0.025 μJ and 0.047 μJ ms for $t_{off} = 15$ ms and $t_{off} = 16$ ms, respectively, Fig. 3a. Due to the higher kinetic energy, ULM descended faster for 15 and 16 ms turn-off time compared to 14 ms turn-off time as seen in Fig. 3c. During $t_{off} = 14$ ms, LLM kinetic energy reduced to approximately 0.0001 μJ, Fig. 3b. Due to late reintroduction of the signal, LLM had moved away from the low-pressure region. Though, LLM opposed the acoustic pressure, it was not able to move upward significantly. Consequently, after the collision, the acoustic pressure failed to hold the merged LM, which continued to move downward in cavity, resulting in outcome 4. For $t_{off} = 16$ ms, kinetic energy of LLM decreased from 0.045 to 0.022 μJ, Fig. 3b. Due to the reduction in kinetic energy, LLM continued moving downward resisting acoustic pressure, Fig. 3d. At the end, ULM and LLM both collapsed in the cavity without coalescence.

Fig. 3e and f illustrate the respective surface energy of ULM and LLM over the first 30 ms for different outcomes. Ideally, at stable levitation and with identical parameters, the surface energies of LMs should be similar. However, during acoustic levitation, minor air perturbation could change the acoustic radiation pressure acting on the LMs, resulting in shape change. As a result, we observed a slight variation in the surface energy of ULM and LLM at stable levitation. The variation in terms of standard deviation was 0.335 μJ for ULM, and 0.242 μJ for LLM. Additionally, as discussed in 2.4, LM had an oblate spheroid shape, which has a higher surface energy compared to the respective volume of the spheroid. Consequently, once the turn-off signal is introduced, both LMs tried to minimise the surface energy, which generated oblate-prolate oscillation of LMs. Due to the oscillation, surface energy also varied accordingly as shown in Fig. 3e and f. From Fig. 3, though the surface energy of LMs was higher than the kinetic energy, gained kinetic energy played an important role in determining the holding ability of LM once the turn-off signal is introduced.

3.3. Operation map of the outcomes

Apart from the turn-off period, we also varied voltage, ULM, and LLM volume. These parameters also played a role in determining the outcomes. Fig. 4 shows the operational map of the coalesce process, illustrating the outcomes based on variations of all parameters. Since outcomes 1, 4, and 5 did not result in coalescence or stable holding within the cavity, only three samples were collected at the observation point. In contrast, five samples were collected for outcomes 2 and 3 to assess the validity of these results. The superscript above outcomes 2 and 3 indicates the number of occurrences out of the five samples, Fig. 4. For a 13 ms turn-off period, outcome 1 consistently occurred regardless of changes in voltage, ULM, and LLM volumes, Fig. 4. Similarly, outcome 5 was observed across various voltages, ULM, and LLM volumes at a 16 ms turn-off period, Fig. 4.

For a 3 μL LLM, acoustic pressures of 10, 10.5, and 11 V successfully counteracted the kinetic energy of the 5 μL and 6 μL ULM, resulting in outcome 1 for a 14-ms turn-off time, Fig. 4a and b. While for the 3 μL LLM and 7 μL ULM, the kinetic energy was sufficiently reduced only for higher acoustic pressure 10.5 and 11 V, which led to outcome 1 for a 14 ms turn-off time, Fig. 4c. At 10 V, the combination of 7 μL ULM and 3 μL LLM resulted in outcome 4, indicating that the acoustic pressure was inadequate to maintain stability post-coalescence, Fig. 4c. For the 5 μL ULM and 3 μL LLM combination, applying 15 ms turn-off signal, all samples exhibited outcome 2 at 10 V, Fig. 4a. In contrast, 3 μL LLM and 6 μL and 7 μL ULMs ended up in outcome 4, indicating insufficient acoustic pressure to hold them post-coalescence, Fig. 4b and c. For 15-ms turn-off period, higher pressures at 10.5 and 11 V resulted in outcome 1 for the 5 μL ULM and 3 μL LLM, Fig. 4a. For 6 μL ULM and 3 μL LLM, three samples showed outcome 2 and two outcome 3 at 10.5 V. At 11 V, one sample showed outcome 2, and four resulted in outcome 3, Fig. 4b. When the ULM volume increased by 1 μL for 3 μL LLM volume and 15 ms turn-off signal, one sample resulted in outcome 2, while four samples resulted in outcome 3 at 10.5 V, Fig. 4c. For same LMs volumes and turn-off signal, all samples resulted in outcome 3 at 11 V, Fig. 4c.

Coalescence (outcome 2) and partial coalescence (outcome 3) occurred despite keeping all parameters constant. In the previous section, we found that higher kinetic energy led to partial coalescence instead of coalescence. Apart from that, two more factors could cause this discrepancy. Previous studies have shown that oblique collisions of LMs can introduce extra shear stress, affecting coalescence behaviour [41,54]. In our study, we couldn't control the offset ratio during LM collisions, making oblique collision a likely cause. Additionally, the arrangement of hydrophobic powder on the LMs was random. In addition, acoustic pressure also influenced the powder's distribution on the liquid surface [55]. In principle, LM with more layers required more energy to break its protective layer. The loss of energy to overcome the extra protective layer might lead to less spreading after coalescence, prevented buckling, and resulted in coalescence (outcome 2). In-depth study and characterisation of both reasons is out of the scope of this

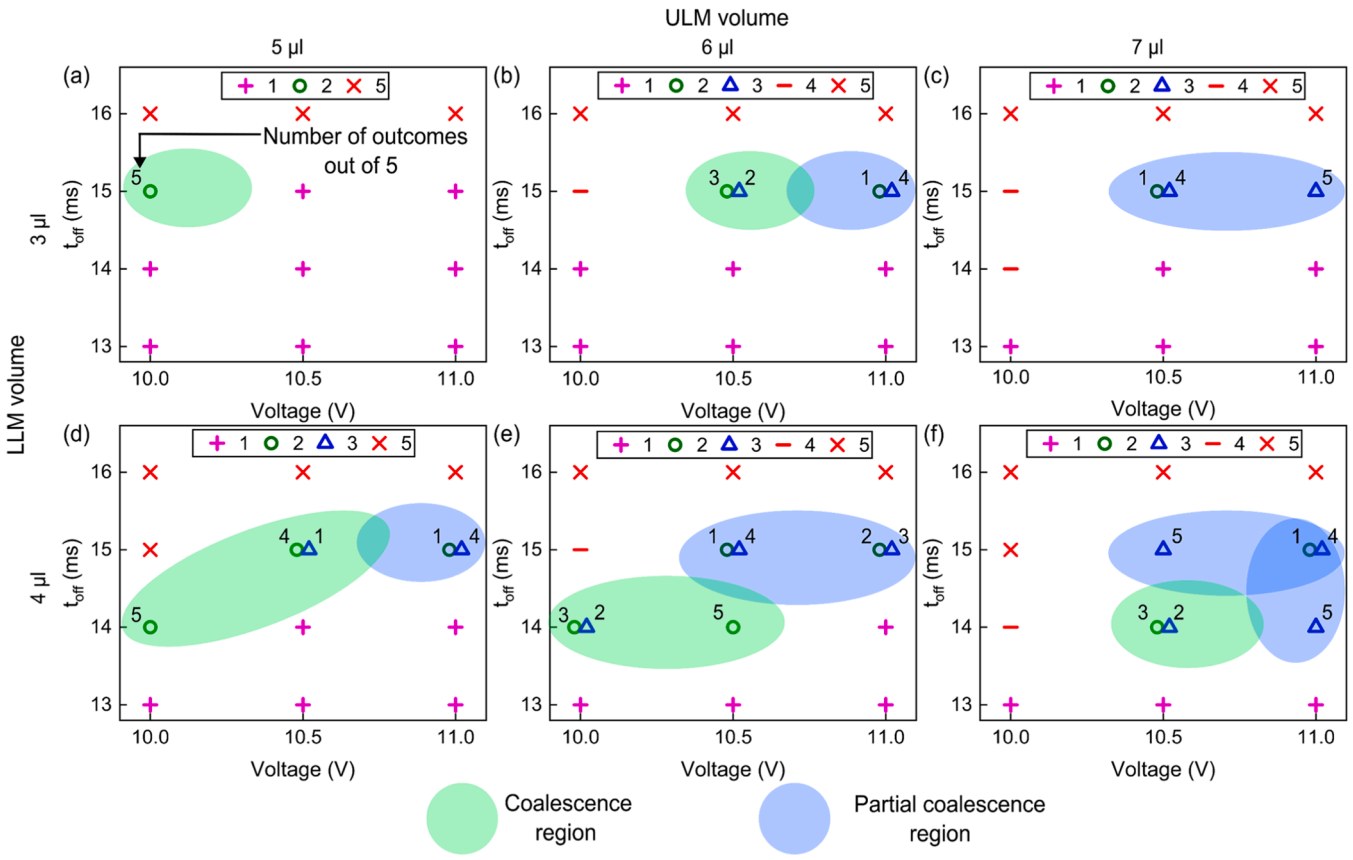

Fig. 4. Operation map depicting the outcomes for varied voltages, turn-off time. For (a), (b), and (c) LLM volume is 3 µl and ULM volume is 5,6, and 7 µl respectively. For (d), (e), and (f) LLM volume is 4 µl and ULM volume is 5,6, and 7 µl respectively. Subscripts showed the number of outcomes out of 5. Coalescence and partial coalescence regions were defined based on the number of outcomes.

paper.

At 10 V with a 4 µL LLM and a 14-ms turn-off period, outcome 2 was achieved for 5 µL ULM, Fig. 4d. For 6 µL ULM, three samples resulted in outcome 2 and two in outcome 3, while for 7 µL LLM the coalesced LM dropped in the levitator, Fig. 4e and f. Increasing 1 ms in turn-off period at same voltage and LLM volume, both LM fell in the cavity after coalescence for 6 µL ULM and without coalescence for 5 µL and 7 µL ULM, Fig. 4d, e and f. Both 5 µL ULM and 4 µL LLM were able to hold their position at 10.5 and 11 V for 14-ms turn-off period, Fig. 4d. Under similar conditions at 10.5 V, four samples resulted in outcome 2 and one in outcome 3, while at 11 V, there was one outcome 2 and four outcome 3 for a 15 ms turn-off period, Fig. 4d. All samples obtained outcome 2 at 10.5 V and outcome 1 at 11 V for 6 µL ULM and 4 µL LLM when the turn-off duration was 14 ms, Fig. 4e. When the turn-off duration was extended to 15 ms, the numbers of outcome 2 and 3 emerged as 1 and 4, 2 and 3 at 10.5 and 11 V, respectively, Fig. 4e. For the 7 µL ULM and 4 µL LLM, three samples showed outcome 2 and two showed outcome 3 at 10.5 V, whereas At 11 V, all samples exhibited in outcome 3 for a 14 ms turn-off period, Fig. 4f. Extending the turn-off period by 1 ms, with LM volumes unchanged, exhibited in outcome 3 at 10.5 V and one outcome 2 and four outcome 3 at 11 V, Fig. 4f.

We further divided the operation map into coalescence and partial coalescence regions based on the number of outcomes, Fig. 4. The coalescence region was identified where outcome 2 occurred more frequently than outcome 3, while the partial coalescence region had a higher numbers of outcome 3. Two main findings emerged from this analysis. First, as the ULM volume increased, the partial coalescence region expanded. This was due to the larger surface area of the LM, leading to greater spreading upon collision. Second, the partial coalescence region also grew with increasing voltage. This can be attributed to the effect of acoustic radiation pressure, which compressed the coalesced LM more at the polar areas under higher acoustic pressure [50]. The increased compression caused the LM to spread more, resulting in buckling and partial coalescence. Therefore, achieving full coalescence required lower ULM volumes and voltages.

3.4. Symmetric Weber number for LM coalescence

The coalescence of LMs was caused by the kinetic energy overcoming the surface energy of LMs. The dimensionless relationship between kinetic and surface energy is represented by Weber number (*We*),

$$We = \frac{E_k}{E_s} \tag{8}$$

In our study, kinetic energy was influenced in the presence of acoustic pressure. Moreover, both LMs has a momentum during collision. Additionally, surface energy of the LMs also varies due to the shape oscillation of LMs. Therefore, to properly characterise the coalescence with dimensionless number, we calculated symmetric Weber number (We_s) at impact [56]. Assuming droplets are impacting vertically with an impact velocity v_i, the symmetric weber number can be calculated as,

$$We_s = \frac{\frac{1}{2}\rho_m V_{(ulm)} u^2_{(ulm)} + \frac{1}{2}\rho_m V_{(llm)} u^2_{(llm)}}{E_{s(ulm)} + E_{s(llm)}} \tag{9}$$

where $u_{(ulm)}$ and $u_{(llm)}$ are relative velocities to the centre of the mass of the incoming droplet. $u_{(ulm)}$ and $u_{(llm)}$ cab be given as $u_{(ulm)} = v_{i(ulm)} - v_g$ and $u_{(llm)} = v_{i(llm)} - v_g$, where v_g represents velocity of the centre of mass and can be obtained by momentum balance [56],

$$V_{(ulm)} v_{i(ulm)} + V_{(llm)} v_{i(llm)} = \left(V_{(ulm)} + V_{(llm)}\right) v_g \tag{10}$$

3.5. Dimensionless regime map of LM coalescence

Fig. 5 presents a dimensionless regime map illustrating the coalescence and partial coalescence based on the symmetric Weber number and the volume ratio between the upper and lower liquid marbles (V_{ULM}/V_{LLM}) across various voltages. In this map, the turn-off period was excluded, as variations in turn-off period primarily influenced the kinetic energy of the LM, which was accounted for in the symmetric Weber number. According to Fig. 5, symmetric Weber number ranged from 0 to 0.03 for different voltages and LM volume ratios. At 10 V, outcomes 2 and 3 occurred for three volume ratios 1.25, 1.5, and 1.67, Fig. 5a. Whereas, at 10.5 V and 11 V, these outcomes were observed for a broader range of ratios 1.25, 1.5, 1.75, 2, and 2.33, Figs. 5b and 5c. In Fig. 5a, variations in the symmetric Weber number and LM volume ratio had minimal effect on the outcome, with most outcomes resulted in full coalescence. At 10.5 V, full coalescence was more likely when the symmetric Weber number was below 0.0025, while values above 0.0025 predominantly lead to partial coalescence with different volume ratios, Fig. 5b. Notably, at the higher acoustic pressure with 11 V, partial coalescence took place even at very low Weber numbers, Fig. 5c. Overall, this regime map demonstrated the impact of acoustic pressure on the outcomes. The higher acoustic pressure resulted in a stronger acoustic radiation force on the LM surface, which induced greater spreading and buckling of the LM, consequently leading to partial coalescence at lower symmetric Weber number.

3.6. Comparison with vertical coalescence study

Caution should be taken while comparing these results with other approaches, as variation in powder coating inherently influence the outcomes. However, some interesting observation can be made with the comparison of Weber number. In previous vertical coalescence study without acoustic levitation, Jin et al. reported modified Weber number of 0.581 or more is required to induce coalescence [41]. The LM with less modified Weber number was not able to break the protective layer and resulted in rebound. The modified Weber number can be converted to the widely used Weber number (We) by multiplying it with 12, yielding a calculated equivalent of 6.972. For our study, the relation between symmetric Weber number and Weber number is given by,

$$We_s = We\frac{\Delta^2}{12\quad(1+\Delta^3)(1+\Delta^2)} \tag{11}$$

where Δ is the ratio of LMs diameter (d_{LLM}/d_{ULM}). Based on this equation, the variation of Weber number in our study for LMs coalescence or partial coalescence is between 0 and 1.589 which is lower than the previous study. Moreover, in Jin et al. study for 5 µl LMs volume, coalescence only occurred in oblique collision [41]. In this study, we successfully achieved the coalescence of a 5 µl ULM and a 3 µl LLM without controlling the direction of their head-on collision. These findings indicate that acoustic pressure in acoustic levitation can effectively drive head-on coalescence without any constraints.

3.7. Future outlook and applications

For the first time, we demonstrated a contactless, cost-effective, and easy to implement method to merge LMs in the vertical direction using acoustic levitation. This method was achieved by employing an Arduino UNO microcontroller with TinyLev system to superimpose a turn-off signal, interrupting the continuous acoustic field. Arduino UNO is versatile microcontroller which provide flexibility to interrupt the continuous field as required. Interrupting the signal more than one time may enable other manipulation techniques, such as controlled transport, splitting, and shape oscillations in LMs. Additionally, the standing wave in TinyLev generates multiple nodes, making it possible to coalesce more than two LMs simultaneously if the superimposed signal is properly controlled. However, caution must be exercised in selecting the volume of the LMs. Larger LMs require higher acoustic pressure to remain stable within the cavity. When merging under these conditions, the increased acoustic radiation pressure due to higher acoustic pressure can lead to greater surface instability, making the LMs more prone to buckling and resulting in partial coalescence.

This study focuses solely on one type of particle for LM coalescence. Variations in particle size could lead to different coalescence outcomes under the same parameters. Therefore, our method also provides a foundation for exploring the effects of particle properties on LM coalescence. Additionally, our method is not limited to LMs but extends to manipulation of any digital microfluidic platforms, makes it perfect method to achieve contact-free digital microfluidics applications on earth similar to outer space. One of the major applications in digital microfluidics is chemical and biochemical reaction. The reaction can be achieved by direct inserting the other liquid with a syringe or a micro pipette [57], or through coalescence [38]. However, direct insertion is invasive which increases the chances of cross contamination. Contrary, coalescence is more controlled and non-invasive which makes the process free of contamination. Using our method for coalescence of LMs provides ultra clean environment for chemical reaction as there is no surface involvement. With acoustic levitation, researchers have achieved extraordinary stability of bubble which can last for several minutes, while enhancing the adsorption of particles [58,59]. Moreover, bubble made composite liquid film so called as gas marble can retain their integrity over year [60,61]. Our method offers the potential generation of these type of bubbles during buckling which can advance the research in bubble dynamics and its applications. In summary, our method opens new possibilities for a wide range of digital microfluidics application.

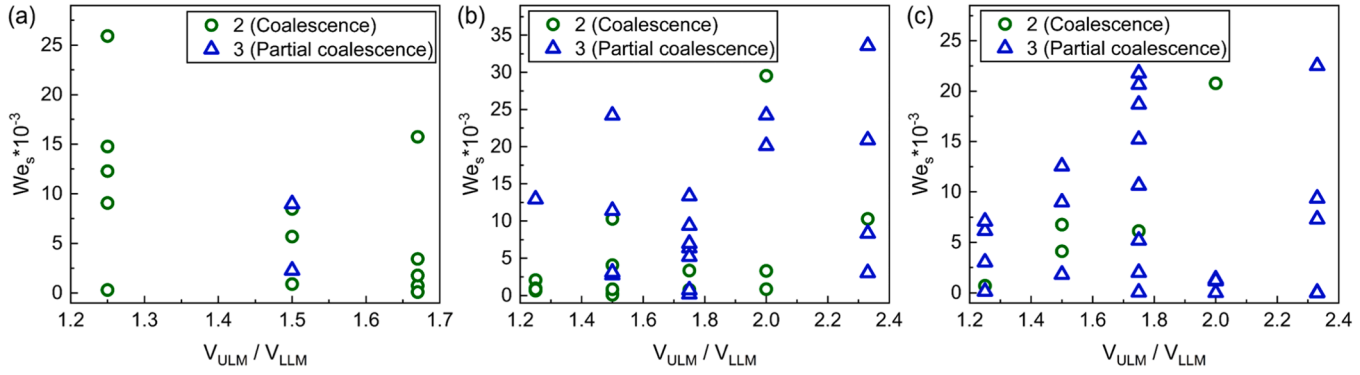

Fig. 5. Dimensionless regime map of liquid marble coalescence with symmetric Weber number and liquid marble volume ratio for varied voltages (a) 10 V, (b) 10.5 V, and (c)11 V.

4. Conclusion

In this study, we examined the head-on coalescence of LMs coated with 1-μm PTFE particles by turning off the levitator for a short period. We distinguished the five different outcomes based on LM holding and merging capability in the acoustic levitator. Next, we evaluated effect of LMs volume, time of turn-off period, and driving voltage on the outcomes. For given LM volumes and voltage range, coalescence or partial coalescence occurred within a 13–16 ms turn-off window. At a turn-off time of 13 ms, both LMs remained in their positions, whereas at 16 ms, both LMs dropped into the cavity. Based on the outcomes, we classified them into distinct regions of coalescence and partial coalescence. The regions revealed that smaller ULM volumes and lower driving voltages significantly increased the probability of full coalescence, while larger ULM volumes and higher driving voltages predominantly led to partial coalescence. Finally, we analysed a dimensionless regime map using the symmetric Weber number and the LM volume ratio across different voltages for coalescence and partial coalescence outcomes. We also compared our results with past LMs vertical coalescence study. The regime map and comparison unveiled the significant role of acoustic pressure in achieving coalescence and partial coalescence outcomes. The method presented in this paper successfully demonstrates head-on, contactless LM coalescence using acoustic levitation for the first time, highlighting its potential for controlled, efficient, and cost-effective LMs manipulation in a contactless manner. Additionally, our results also provide valuable insights into selecting optimal parameters to facilitate micro reactions in an acoustic levitator without liquid loss.

CRediT authorship contribution statement

Yadav Ajeet Singh: Visualization, Formal analysis. **Kashaninejad Navid:** Writing – review & editing, Supervision. **Vashi Aditya:** Writing – original draft, Visualization, Investigation, Formal analysis, Conceptualization. **Nguyen Nam-Trung:** Writing – review & editing, Supervision, Conceptualization.

Declaration of Competing Interest

The authors declare that they have no known competing financial interests or personal relationships that could have appeared to influence the work reported in this paper.

Acknowledgements

The authors are grateful to Griffith University for providing facilities to carry out the research. A.V. is grateful for the funding and support from the Griffith University International Postgraduate Research Scholarship. N.K. acknowledges funding support from the Australian Research Council (ARC) through the Discovery Early Career Research Award (DECRA) DE220100205.

Data availability

Data will be made available on request.

References

[1] C. Gonzalez-Ballestero, et al., Levitodynamics: levitation and control of microscopic objects in vacuum, Science 374 (6564) (2021) eabg3027.
[2] M.A.B. Andrade, N. Pérez, J.C. Adamowski, Review of progress in acoustic levitation, Braz. J. Phys. 48 (2) (2018) 190–213.
[3] H. Chen, Z. Hong, D. Zang, New insights into suspended drops: when soft matter meets acoustic levitation, Droplet 3 (1) (2024) e95.
[4] D. Geng, et al., Extraordinary solidification mechanism of liquid alloys under acoustic levitation state, Adv. Mater. (2022) 2206464.
[5] S. Santesson, S. Nilsson, Airborne chemistry: acoustic levitation in chemical analysis, Anal. Bioanal. Chem. 378 (7) (2004) 1704–1709.
[6] C.J. Benmore, J.K.R. Weber, Amorphization of molecular liquids of pharmaceutical drugs by acoustic levitation, Phys. Rev. X 1 (1) (2011) 011004.
[7] A. Vashi, et al., Parametric analysis of acoustically levitated droplet for potential microgravity application, Appl. Acoust. 213 (2023) 109624.
[8] J.G. McDaniel, R.G. Holt, Measurement of aqueous foam rheology by acoustic levitation, Phys. Rev. E 61 (3) (2000) R2204–R2207.
[9] A. Kundt, Ueber eine neue Art akustischer Staubfiguren und über die Anwendung derselben zur Bestimmung der Schallgeschwindigkeit in festen Körpern und Gasen, Ann. der Phys. 203 (4) (1866) 497–523.
[10] J.K.R. Weber, et al., Acoustic levitator for structure measurements on low temperature liquid droplets, Rev. Sci. Instrum. 80 (8) (2009) 083904.
[11] M.A.B. Andrade, T.S.A. Camargo, A. Marzo, Automatic contactless injection, transportation, merging, and ejection of droplets with a multifocal point acoustic levitator, Rev. Sci. Instrum. 89 (12) (2018).
[12] C. Shen, W. Xie, B. Wei, Parametrically excited sectorial oscillation of liquid drops floating in ultrasound, Phys. Rev. E 81 (4) (2010) 046305.
[13] R. Gunn, Collision characteristics of freely falling water drops, Science 150 (3697) (1965) 695–701.
[14] F. Raes, R. Van Dingenen, Simulations of condensation and cloud condensation nuclei from biogenic SO2 in the remote marine boundary layer, J. Geophys. Res. Atmospheres 97 (D12) (1992) 12901–12912.
[15] F. Raes, et al., Formation and cycling of aerosols in the global troposphere, Atmos. Environ. 34 (25) (2000) 4215–4240.
[16] Y.H. Kim, et al., Controlled deposition of a high-performance small-molecule organic single-crystal transistor array by direct ink-jet printing, Adv. Mater. 24 (4) (2011) 497–502.
[17] K.A. Estes, I. Mudawar, Correlation of Sauter mean diameter and critical heat flux for spray cooling of small surfaces, Int. J. Heat. Mass Transf. 38 (16) (1995) 2985–2996.
[18] C.T. Bellehumeur, M. Bisaria, J. Vlachopoulos, An experimental study and model assessment of polymer sintering, Polym. Eng. Sci. 36 (17) (1996) 2198–2207.
[19] T. Dreher, et al., Effect of rheology on coalescence rates and emulsion stability, AIChE J. 45 (6) (1999) 1182–1190.
[20] D. Foresti, et al., Acoustophoretic contactless transport and handling of matter in air, Proc. Natl. Acad. Sci. 110 (31) (2013) 12549–12554.
[21] A. Watanabe, K. Hasegawa, Y. Abe, Contactless fluid manipulation in air: Droplet coalescence and active mixing by acoustic levitation, Sci. Rep. 8 (1) (2018) 10221.
[22] K. Hasegawa, A. Watanabe, Y. Abe, Acoustic manipulation of droplets under reduced gravity, Sci. Rep. 9 (1) (2019) 16603.
[23] K. Hasegawa, et al., Coalescence dynamics of acoustically levitated droplets, Micromachines 11 (4) (2020) 343.
[24] S.J. Brotton, R.I. Kaiser, Controlled chemistry via contactless manipulation and merging of droplets in an acoustic levitator, Anal. Chem. 92 (12) (2020) 8371–8377.
[25] A. Vashi, et al., The dynamics of vertical coalescence of acoustically levitated droplets, Microfluid. Nanofluidics 28 (5) (2024) 34.
[26] P. Aussillous, D. Quéré, Liquid marbles, Nature 411 (6840) (2001) 924–927.
[27] D.-G. Lee, H.-Y. Kim, Impact of a superhydrophobic sphere onto water, Langmuir 24 (1) (2008) 142–145.
[28] E. Bormashenko, R. Pogreb, A. Musin, Stable water and glycerol marbles immersed in organic liquids: from liquid marbles to Pickering-like emulsions, J. Colloid Interface Sci. 366 (1) (2012) 196–199.
[29] Y. Xue, et al., Magnetic liquid marbles: a “precise” miniature reactor, Adv. Mater. 22 (43) (2010) 4814–4818.
[30] E. Bormashenko, R. Balter, D. Aurbach, Micropump based on liquid marbles, Appl. Phys. Lett. 97 (2010) 9.
[31] J. Tian, et al., Liquid marble for gas sensing, Chem. Commun. 46 (26) (2010) 4734–4736.
[32] C.H. Ooi, N.-T. Nguyen, Manipulation of liquid marbles, Microfluid. Nanofluidics 19 (2015) 483–495.
[33] J. Jin, N.-T. Nguyen, Manipulation schemes and applications of liquid marbles for micro total analysis systems, Microelectron. Eng. 197 (2018) 87–95.
[34] X. Ji, et al., Interfacial viscoelasticity and jamming of colloidal particles at fluid–fluid interfaces: a review, Rep. Prog. Phys. 83 (12) (2020) 126601.
[35] Y. Feng, et al., Effect of surface roughness on the solar evaporation of liquid marbles, J. Colloid Interface Sci. 629 (2023) 644–653.
[36] Y. Feng, et al., Effect of particle size on the stripping dynamics during impact of liquid marbles onto a liquid film, Soft Matter 18 (28) (2022) 5230–5238.
[37] J.R. Dorvee, et al., Manipulation of liquid droplets using amphiphilic, magnetic one-dimensional photonic crystal chaperones, Nat. Mater. 3 (12) (2004) 896–899.
[38] Z. Liu, et al., Coalescence of electrically charged liquid marbles, Soft Matter 13 (1) (2017) 119–124.
[39] B. Wang, et al., On-demand coalescence and splitting of liquid marbles and their bioapplications, Adv. Sci. 6 (10) (2019) 1802033.
[40] C. Planchette, et al., Coalescence of armored interface under impact, Phys. Fluids 25 (4) (2013).
[41] J. Jin, et al., Liquid marble coalescence via vertical collision, Soft Matter 14 (20) (2018) 4160–4168.
[42] Z. Chen, et al., Liquid marble coalescence and triggered microreaction driven by acoustic levitation, Langmuir 33 (25) (2017) 6232–6239.
[43] P. Aussillous, D. Quéré, Properties of liquid marbles, Proc. R. Soc. A Math. Phys. Eng. Sci. 462 (2067) (2006) 973–999.
[44] A. Marzo, A. Barnes, B.W. Drinkwater, TinyLev: a multi-emitter single-axis acoustic levitator, Rev. Sci. Instrum. 88 (8) (2017) 085105.

[45] M.J. Akbari, M.A. Bijarchi, M.B. Shafii, Experimental investigation on the bouncing dynamics of a liquid marble during the impact on a hydrophilic surface, J. Colloid Interface Sci. 662 (2024) 637–652.
[46] P. Singha, et al., Capillarity: revisiting the fundamentals of liquid marbles, Microfluid. Nanofluidics 24 (10) (2020) 81.
[47] T. Arbatan, W. Shen, Measurement of the surface tension of liquid marbles, Langmuir 27 (21) (2011) 12923–12929.
[48] T. Supakar, A. Kumar, J.O. Marston, Impact dynamics of particle-coated droplets, Phys. Rev. E 95 (1) (2017) 013106.
[49] L.V. King, On the acoustic radiation pressure on spheres, Proc. R. Soc. Lond. Ser. A Math. Phys. Sci. 147 (861) (1934) 212–240.
[50] D. Zang, et al., Inducing drop to bubble transformation via resonance in ultrasound, Nat. Commun. 9 (1) (2018) 3546.
[51] A. Vashi, A.S. Yadav, N.-T. Nguyen, Micro container made of levitated liquid bead, Colloids Surf. A Physicochem. Eng. Asp. 702 (2024) 135185.
[52] H.T. O'Neil, Theory of focusing radiators, J. Acoust. Soc. Am. 21 (5) (1949) 516–526.
[53] A.S. Basu, Droplet morphometry and velocimetry (DMV): a video processing software for time-resolved, label-free tracking of droplet parameters, Lab a Chip 13 (10) (2013) 1892–1901.
[54] T.C. Draper, et al., Mapping outcomes of liquid marble collisions, Soft Matter 15 (17) (2019) 3541–3551.
[55] D. Zang, et al., Switchable opening and closing of a liquid marble via ultrasonic levitation, Langmuir 31 (42) (2015) 11502–11507.
[56] C. Rabe, J. Malet, F. Feuillebois, Experimental investigation of water droplet binary collisions and description of outcomes with a symmetric Weber number, Phys. Fluids 22 (4) (2010).
[57] E.S. Lin, et al., Liquid marble clearance and restoration via gas bubble insertion and bursting, Soft Matter 17 (9) (2021) 2512–2517.
[58] X. Ji, et al., Toward enhanced aerosol particle adsorption in never-bursting bubble via acoustic levitation and controlled liquid compensation, Adv. Sci. 10 (19) (2023) 2300049.
[59] X. Ji, et al., Extraordinary stability of surfactant-free bubbles suspended in ultrasound, Droplet 3 (2) (2024) e119.
[60] Y. Timounay, O. Pitois, F. Rouyer, Gas marbles: much stronger than liquid marbles, Phys. Rev. Lett. 118 (22) (2017) 228001.
[61] A. Roux, A. Duchesne, M. Baudoin, Everlasting bubbles and liquid films resisting drainage, evaporation, and nuclei-induced bursting, Phys. Rev. Fluids 7 (1) (2022) L011601.